



Cite this: *Nanoscale Adv.*, 2023, 5, 2038

Received 25th October 2022  
Accepted 22nd February 2023

DOI: 10.1039/d2na00744d  
[rsc.li/nanoscale-advances](http://rsc.li/nanoscale-advances)

## Continuous manufacturing of highly stable lead halide perovskite nanocrystals *via* a dual-reactor strategy†

Shuang Liang,<sup>‡ab</sup> Gill M. Biesold,<sup>‡a</sup> Mingyue Zhuang,<sup>‡ad</sup> Zhitao Kang,<sup>\*c</sup> Brent Wagner<sup>c</sup> and Zhiqun Lin <sup>ID</sup> <sup>\*ad</sup>

Lead halide perovskite nanocrystals possess incredible potential as next generation emitters due to their stellar set of optoelectronic properties. Unfortunately, their instability towards many ambient conditions and reliance on batch processing hinder their widespread utilities. Herein, we address both challenges by continuously synthesizing highly stable perovskite nanocrystals *via* integrating star-like block copolymer nanoreactors into a house-built flow reactor. Perovskite nanocrystals manufactured in this strategy display significantly enhanced colloidal, UV, and thermal stabilities over those synthesized with conventional ligands. Such scaling up of highly stable perovskite nanocrystals represents an important step towards their eventual use in many practical applications in optoelectronic materials and devices.

## Introduction

Metal halide perovskites, with the general structure  $ABX_3$ , have recently been recognized for their tremendous potential in optoelectronic applications, including LEDs,<sup>1,2</sup> photodetectors,<sup>3,4</sup> scintillators,<sup>5,6</sup> solar cells,<sup>7–9</sup> etc. Lead halide perovskite nanocrystals (PNCs) have been demonstrated to possess an array of intriguing optical properties,<sup>10</sup> including a high photoluminescence quantum yield (PLQY),<sup>11–13</sup> narrow full width at half maximum of emission (FWHM),<sup>14,15</sup> widely tunable emission wavelength,<sup>5,16</sup> and high defect tolerance.<sup>17,18</sup> Additionally, PNCs can be synthesized at room temperature under ambient conditions,<sup>19–21</sup> which stands in stark contrast to the air-free and high temperature synthesis conditions needed for conventional semiconductor quantum dots (*i.e.* CdSe,<sup>22</sup> PbSe,<sup>23</sup> CdTe<sup>24</sup>). Despite these encouraging properties, their widespread use remains hindered by their poor overall stability and their reliance on batch processing techniques. In particular, PNCs demonstrate poor moisture,<sup>25</sup> thermal,<sup>26</sup> and UV<sup>27</sup> stabilities. PNCs also often suffer from poor colloidal stability due to the dynamic bonding nature of conventional ligands (usually oleic

acid and oleylamine).<sup>28</sup> Additionally, PNCs are most often synthesized through batch techniques (*e.g.* hot injection<sup>29</sup> and ligand assisted reprecipitation (LARP)<sup>21,30</sup>), and while these methods produce high-quality PNCs, a shift towards continuous manufacturing is needed to realize their commercial potential.

Numerous methods have been used to increase the stability of PNCs, including incorporation of PNCs in silica,<sup>31</sup> alumina,<sup>32</sup> zinc stearate.<sup>33</sup> Integrating PNCs with a variety of polymer matrixes has also been demonstrated to improve stability.<sup>34</sup> One of the most promising techniques to synthesize highly stable colloidal PNCs is to capitalize on amphiphilic star-like block copolymers as templates.<sup>35–37</sup> These nanoreactors are comprised of inner poly(acrylic acid) (PAA) and outer polystyrene (PS) blocks and form unimolecular micelles in solution state. The inner PAA blocks can coordinate with perovskite precursors to template nanocrystal growth, while the outer PS blocks enable solubility in organic solvents. Notably, these PS chains are permanently ligated to the surface of the nanocrystals *via* their covalent bonded with the inner PAA blocks.<sup>38</sup> The permanence of these ligated chains imparts better colloidal stability than that is afforded by the dynamically bound ligands in conventional colloidal synthesis.<sup>39</sup>

To promote perovskite nanomaterials towards commercialization, progress beyond batch synthesis is highly desirable. Some pioneering works have developed continuous manufacturing techniques.  $CsPbX_3$  (ref. 40 and 41) and  $FAPbX_3$  (ref. 42) PNCs have been synthesized using microfluidic flow systems, where precursor solutions were mixed in droplets dispersed in an inert oil medium.  $Cs_4PbBr_6$  PNCs with excellent optical properties were synthesized using an apparatus consisting of concentric rotating cylinders that resulted in Couette-

<sup>a</sup>School of Materials Science and Engineering, Georgia Institute of Technology, Atlanta 30332, GA, USA

<sup>b</sup>School of Chemical and Biomolecular Engineering, Georgia Institute of Technology, Atlanta 30332, Georgia, USA

<sup>c</sup>Georgia Tech Research Institute, Georgia Institute of Technology, Atlanta 30332, Georgia, USA. E-mail: [zhitao.Kang@gtri.gatech.edu](mailto:zhitao.Kang@gtri.gatech.edu)

<sup>d</sup>Department of Chemical and Biomolecular Engineering, National University of Singapore, Singapore 117585, Singapore. E-mail: [z.lin@nus.edu.sg](mailto:z.lin@nus.edu.sg)

† Electronic supplementary information (ESI) available. See DOI: <https://doi.org/10.1039/d2na00744d>

‡ Co-first authors.



Taylor flow.<sup>43</sup> MAPbX<sub>3</sub> PNCs have also been synthesized using conventional flow reactors.<sup>44,45</sup> In a previous work, we developed a flow reactor system to synthesize high PLQY 2D (PEA)<sub>2</sub>PbX<sub>4</sub> (PEA = phenylethylammonium, X= Br, I) Ruddlesden–Popper perovskite nanoplatelets.<sup>46</sup> Notably, while all these continuous production methods can manufacture high-quality PNCs, the final products still suffer from perovskite's characteristic poor environmental stabilities. Thus, the continuous production of stable PNCs remains an urgent need, and the integration of novel star-like block copolymer nanoreactors into flow reactors offers an exciting solution to this end.

Herein, we demonstrate the continuous synthesis of highly stable PNCs by incorporating amphiphilic star-like block copolymer nanoreactors into a continuous flow reactor. Such amphiphilic star-shaped block copolymers are first synthesized by sequential atom transfer radical polymerization (ATRP) of brominated  $\beta$ -cyclodextrin macroinitiators. These nanoreactors are then loaded with perovskite precursors and introduced into a house-built flow reactor. The synthesis of PNCs was then optimized by first surveying the ideal antisolvent for high quality PNC formation. The injection flowrate of that antisolvent ( $Q_{\text{antisolvent}}$ ) was then optimized at a fixed precursor solution injection rate ( $Q_{\text{precursor}}$ ). Subsequently, an ideal  $Q_{\text{precursor}}$  was determined by varying  $Q_{\text{precursor}}$  with  $Q_{\text{antisolvent}}$  held constant. Finally, the optical properties, morphology, and stabilities of the templated PNCs were compared to continuously-produced PNCs synthesized from conventional oleic acid and oleylamine (OA/OAm) ligands. Notably, the templated PNCs displayed a similar PLQY to and significantly enhanced colloidal, UV, and thermal stabilities over the control OA/OAm-co-capped PNCs.

## Results and discussion

As noted above, the use of amphiphilic star-like block copolymer nanoreactors is key to achieving highly stable PNCs. The nanoreactors were synthesized using methods from previous literature,<sup>35,36,47</sup> and detailed procedures to synthesize the star-like block copolymers are available in the ESI.<sup>†</sup> Fig. 1a depicts the route to PNCs by capitalizing on amphiphilic star-like block copolymer as nanoreactor. First, ATRP macroinitiators were synthesized by brominating  $\beta$ -cyclodextrin ( $\beta$ -CD) with  $\alpha$ -bromoisobutyryl bromide (BiBB). Because  $\beta$ -CD possesses seven glucose subunits (and each of those has 3 OH groups), the final brominated  $\beta$ -CD will have 21 bromine terminals for ATRP initiation. Blocks of poly(*tert*-butyl acrylate) (PtBA) were then grown *via* ATRP (upper third panel; Fig. 1a). Once the PtBA blocks were grafted, polystyrene (PS) blocks were subsequently grown from the inner PtBA blocks (upper right panel; Fig. 1a). Afterwards, the inner PtBA was hydrolyzed to form poly(acrylic acid) (PAA) (lower right panel; Fig. 1a). This step is necessary as PAA cannot be directly synthesized *via* ATRP because the carboxyl groups in PAA coordinate too strongly with the necessary copper catalyst, preventing any significant chain growth.<sup>48</sup> The carboxyl groups on the inner PAA blocks have also been demonstrated to coordinate with metal moieties in nanocrystal precursors,<sup>35,36,39,48,49</sup> which enables facile NC formation within

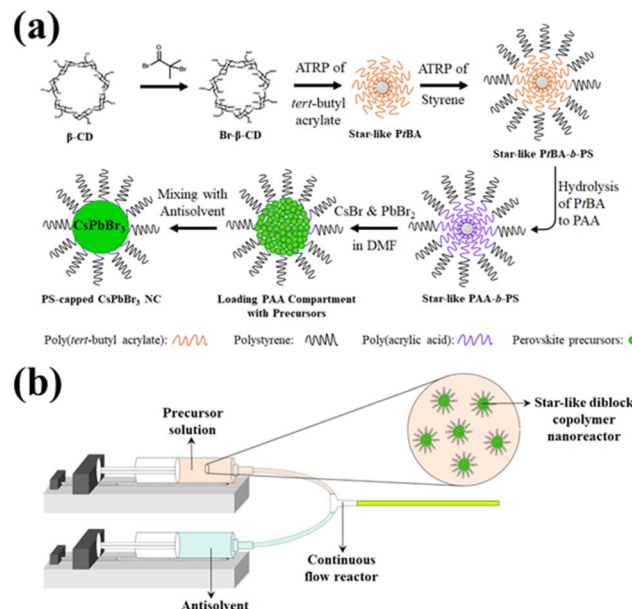


Fig. 1 (a) Stepwise representation of route to star-like PAA-*b*-PS diblock copolymer nanoreactor and the resulting PS-capped CsPbBr<sub>3</sub> nanocrystal. (b) Schematic diagram of dual flow/nano reactor apparatus.

the compartment occupied by PAA blocks of star-like PAA-*b*-PS block copolymer as nanoreactor. Gel permeation chromatography (GPC) traces and proton nuclear magnetic resonance (<sup>1</sup>H-NMR) spectra of each step of the process are shown in Fig. S1 and S2a–c.<sup>†</sup> The complete 21 arm star-like polymer nanoreactors were then dissolved in DMF with perovskite precursors (*i.e.*, PbBr<sub>2</sub> and CsBr) and stirred to allow for coordination of the precursors with the carboxylic acid groups in the PAA. As a result, precursors are confined in the space taken by the PAA core. Once loaded, PNCs can easily be produced (*i.e.*, PS-capped PNC; lower left panel, Fig. 1a) by adding the nanoreactor/perovskite precursor solution (*i.e.*, perovskite precursors-loaded nanoreactor; lower central panel, Fig. 1a) into a nonpolar antisolvent (*e.g.* toluene), spurring crystallization in a modified ligand-assisted reprecipitation (LARP) technique, *i.e.*, precursors quickly coprecipitate in toluene within the inner PAA compartment. The mechanism of the formation of PNC inside the nanoreactors has been detailed in our previous work.<sup>46</sup>

A variety of solvents were explored to determine the ideal antisolvent for PNC synthesis (*i.e.*, CsPbBr<sub>3</sub>). Using a modified LARP technique (noted above), 50  $\mu$ L preloaded nanoreactor solution was dropped into 10 mL vigorously stirring toluene, chlorobenzene, dichloromethane, chloroform, and hexane. The optical properties of the CsPbBr<sub>3</sub> PNCs yielded from this technique were then compared, as seen in Table S1.<sup>†</sup> Using toluene as an antisolvent resulted in PNCs with the highest PLQY, followed by chlorobenzene and chloroform/dichloromethane. Using hexane as an antisolvent did not yield PNCs with any detectable emission. The vastly different properties from each antisolvent can be attributed to the polarity of solvent, which



may cause degradation of perovskite, and interaction of solvent with the outer PS ligands, which may induce incomplete or no crystallization. The ionic crystal nature of perovskite renders them susceptible to be degraded in the presence of polar solvents,<sup>50</sup> leading to the observed drop in PLQY with increasing polarity of solvents (from toluene (9.9) to chlorobenzene (18.8) to dichloromethane (30.9)/chloroform (25.9)).<sup>51</sup> Because chlorobenzene, dichloromethane, and chloroform are good solvents for PS, they can easily reach the surface of the PNC and trigger degradation. The lack of photoluminescent performance from PNCs made with hexane can be ascribed to the fact that PS is insoluble in hexane.<sup>52</sup> For the covalently-bonded outermost polymer block to be effective as permanent ligands, a favorable interaction with the solvent is necessary. As PS is not soluble in hexane, no colloidal nanoparticles could form, only aggregates of perovskite precursors. This small-scale exploration verified that toluene is the best solvent to employ going forward in the flow reactor for continuous synthesis.

To enable continuous production of  $\text{CsPbBr}_3$  PNCs, a house-built flow reactor was constructed, as was reported in our previous work.<sup>46</sup> A diagram of the flow reactor is depicted in Fig. 1b. It consists of two syringe pumps, with Luer lock PTFE tubing connected to the ends of the syringes (one for the precursor solution and another for the antisolvent), and a Y-connector that facilitates mixing of the two solutions. The operating principal of this flow reactor is similar to that of LARP, yet instead of a magnetic stir bar, the mixing is accomplished by the flow dynamics at the Y-connector.<sup>36</sup>

After toluene was selected as the preferred antisolvent, the toluene flowrate ( $Q_{\text{tol}}$ ) for both nanoreactor-enabled PNCs (*i.e.*, PS-capped  $\text{CsPbBr}_3$ ) and conventional ligand-assisted PNCs (*i.e.*, OA/OAm-co-capped  $\text{CsPbBr}_3$  as control sample; see Experimental Section in ESI†) was optimized by varying  $Q_{\text{tol}}$  and holding  $Q_{\text{precursor}}$  at a constant  $60 \text{ mL h}^{-1}$ . For both types of  $\text{CsPbBr}_3$  PNCs, a monotonic increase in PLQY was seen  $Q_{\text{tol}}$  increased from  $1000$  to  $5000 \text{ mL h}^{-1}$  (Fig. 2a). This increased PLQY can probably be attributed to the enhanced mixing of the precursors and antisolvent that occurs at higher flowrates of toluene. The rising flowrates result in an increase in the corresponding Reynolds number from  $394$  (for  $Q_{\text{tol}} = 1000 \text{ mL h}^{-1}$ ) to  $1662$  (for  $Q_{\text{tol}} = 5000 \text{ mL h}^{-1}$ ). The complete calculation of Reynolds number is shown in Table S2.† The transition from laminar Poiseuille flow to turbulent flow in circular tubes is generally accepted to occur at a critical Reynolds number between  $1800$  and  $2300$ .<sup>53,54</sup> While the Reynolds number at the max flowrate still falls within the laminar flow range ( $\text{Re} = 1662 < 1800$ ), the increasing flow has thus been found to promote better mixing.<sup>55</sup> It is notable that the conventionally-ligated PNCs (*i.e.*, OA/OAm-co-capped  $\text{CsPbBr}_3$ ) display a higher average PLQY than those synthesized with the nanoreactor. This is likely due to presence of the PAA blocks inside the template-grown PNCs.<sup>36</sup> While these PAA chains are necessary for the formation of PNCs within the nanoreactor (due to their coordination with perovskite precursors), their presence could also introduce defects into the crystal structure, thus hindering PLQY.<sup>36</sup> It is worth noting that although the PLQY of the pristine  $\text{CsPbBr}_3$  nanoparticles synthesized from nanoreactor is not

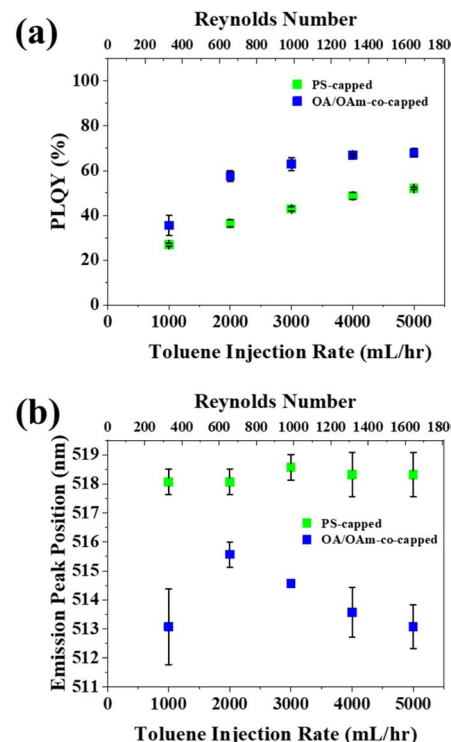


Fig. 2 (a) Effect of  $Q_{\text{toluene}}$  on PLQY and (b) emission peak position of PS-capped  $\text{CsPbBr}_3$  PNCs via capitalizing on star-like PAA-b-PS as nanoreactor and OA/OAm-co-capped  $\text{CsPbBr}_3$  PNCs (control sample).

ideal, it could be improved *via* post-synthesis treatment with zinc bromide to passivate the PS-capped PNC surface.<sup>36</sup> The emission peak position of PS-capped PNCs was unaffected by  $Q_{\text{tol}}$ , whereas the OA/OAm-co-capped PNCs showed a general trend of decreasing peak position with increasing  $Q_{\text{tol}}$  (Fig. 2b). The constant emission peak of PS-capped PNCs can be attributed to the good size control that the star-like PAA-b-PS nanoreactors enable. Because only the PAA blocks coordinate with the perovskite precursors, the size of the PNC is dictated by the length of the inner PAA blocks. The constant emission wavelength of PS-capped PNCs stands in contrast to conventional OA/OAm-co-capped PNCs, which show a general increase in emission peak position as  $Q_{\text{tol}}$  decreased. This red-shifted emission of OA/OAm-co-capped PNCs could be ascribed to an increase of defects in PNCs synthesized at lower flowrates. As discussed above, higher flowrates promote better mixing,<sup>55</sup> thus yielding more crystalline PNCs which lack defects that are known to promote red-shifting of emission.<sup>56,57</sup> We note that OA/OAm-co-capped PNCs made at  $Q_{\text{tol}} = 1000 \text{ mL h}^{-1}$  do not match the trend seen for  $Q_{\text{tol}} = 2000$  through  $5000 \text{ mL h}^{-1}$ . This difference may be due to the extremely low mixing that occurs at  $Q_{\text{tol}} = 1000 \text{ mL h}^{-1}$  ( $\text{Re} = 394$ ).

Following the highest  $Q_{\text{tol}}$  determined to be the most beneficial, we optimized  $Q_{\text{precursor}}$ . To this end,  $Q_{\text{precursor}}$  was varied from  $10$  to  $60 \text{ mL h}^{-1}$ , while keeping  $Q_{\text{tol}}$  constant at  $5000 \text{ mL h}^{-1}$ . Varying  $Q_{\text{precursor}}$  exerted little effect on the PLQY of either PS-capped or OA/OAm-co-capped  $\text{CsPbBr}_3$  PNCs (Fig. 3a). A



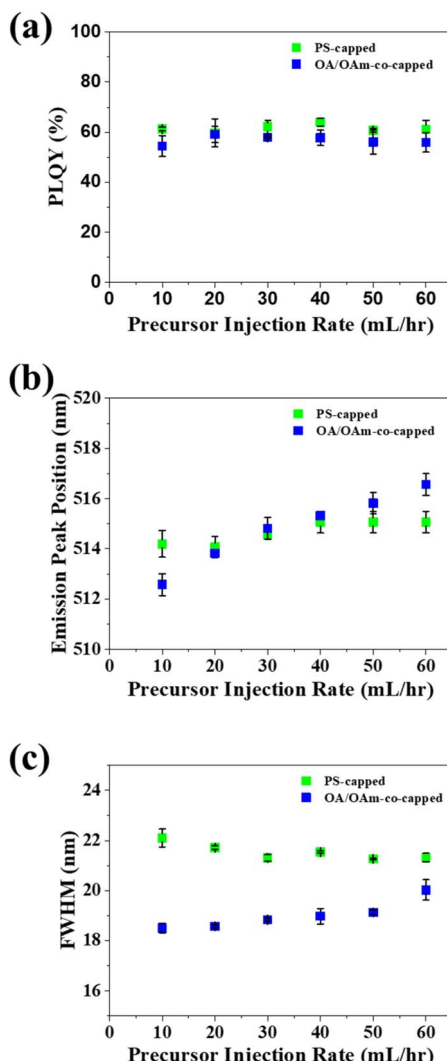


Fig. 3 Effect of  $Q_{\text{precursor}}$  on (a) PLQY, (b) emission peak position, and (c) FWHM of PS-capped  $\text{CsPbBr}_3$  PNCs and OA/OAm-co-capped  $\text{CsPbBr}_3$  PNCs (control sample), where  $Q_{\text{tol}}$  was held constant at the optimized  $5000 \text{ mL h}^{-1}$ .

relatively stable PLQY near 60% was evidenced for both template-grown and control PNCs, signifying that altering the precursor to antisolvent ratio has little impact on the crystal quality. The emission peak position of PS-capped PNCs was constant at all tested  $Q_{\text{precursor}}$ , yet the emission peak of OA/OAm-co-capped PNCs was seen to increase with increasing  $Q_{\text{precursor}}$  (Fig. 3b). This is likely due to the increasing precursor to antisolvent ratio, which favors larger PNCs, leading to less quantum-confinement. The full width of half maximum (FWHM) of the template-grown and control PNCs was relatively unaffected by altering  $Q_{\text{precursor}}$  (Fig. 3c). This suggests that the crystal quality of the PNCs was also unaffected, which is consistent with the stable PLQY observed.<sup>58–61</sup> It is notable that the properties and quality of the PS-capped PNCs showed much weaker dependence on the experimental parameters than the low dimensional perovskite nanocrystals fabricated with the same flow reactor in our previous work. This clearly illustrates

the robustness of the nanoreactor strategy in reliably producing nanoparticles with consistent and controllable properties.

With the optimized conditions (*i.e.*,  $Q_{\text{tol}} = 5000 \text{ mL h}^{-1}$  and  $Q_{\text{precursor}} = 60 \text{ mL h}^{-1}$  to maximize production) for continuous production of PNCs identified, they were used to synthesize  $\text{CsPbBr}_3$  PNCs for further characterization and stability testing. TEM images show that the PS-capped PNCs possessed an average diameter of 13.5 nm (Fig. 4a and b), in good agreement with the calculated diameter using the equation developed in our prior work (eqn S1;  $\dagger$  the calculated radius of gyration  $R_g$  of star-like PAA blocks is 12.9 nm).<sup>62</sup> It is notable that past studies using the nanoreactor have shown that the equation often underestimates the size of the formed nanocrystals.<sup>36</sup> Notably, PS-capped PNCs formed by *via* the nanoreactor strategy are significantly smaller on average (13.5 nm) than those formed with conventional OA and OAm ligands (22 nm) (Fig. 4c and d), even though the amount of perovskite precursors and other experimental methods are identical. This manifests that the star-like PAA-*b*-PS nanoreactor restricts growth of PNC below that which may otherwise be favored. A control experiment was also conducted in which a solution of perovskite precursors ( $\text{CsBr}$  and  $\text{PbBr}_3$ ) was loaded into the flow reactor without the presence of any organic ligands (*i.e.*, no OA and OAm as well as no star-like PAA-*b*-PS nanoreactor). No luminescence was detected for the ligand-free  $\text{CsPbBr}_3$ . This offers further proof to suggest that any luminescent performance from template-grown PNCs can clearly be attributed to  $\text{CsPbBr}_3$  formed within the nanoreactor.

The colloidal, UV, and thermal stabilities of control and templated  $\text{CsPbBr}_3$  PNCs were then examined. In colloidal stability testing, the templated PNCs exhibited nearly no PLQY deterioration over more than 100 days, while the control falls to 20% normalized PLQY (Fig. 5a). The significantly enhanced colloidal stability of the templated PNCs is due to their strongly ligated outer PS chains that are originally covalently bound to the inner PAA chains. Conventional OA and OAm ligands are only dynamically bound to the surface of the PNC, and over time

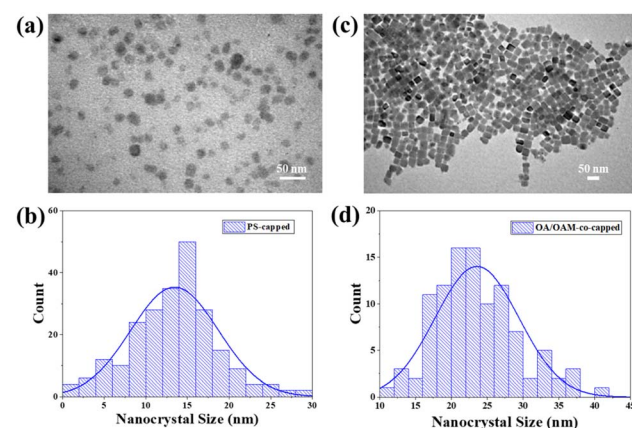


Fig. 4 TEM image and size distribution of (a and b) PS-capped  $\text{CsPbBr}_3$  PNCs and (c and d) OA/OAm-co-capped  $\text{CsPbBr}_3$  PNCs (control sample). Both samples were synthesized at optimized conditions ( $Q_{\text{tol}} = 5000 \text{ mL h}^{-1}$  and  $Q_{\text{precursor}} = 60 \text{ mL h}^{-1}$ ).

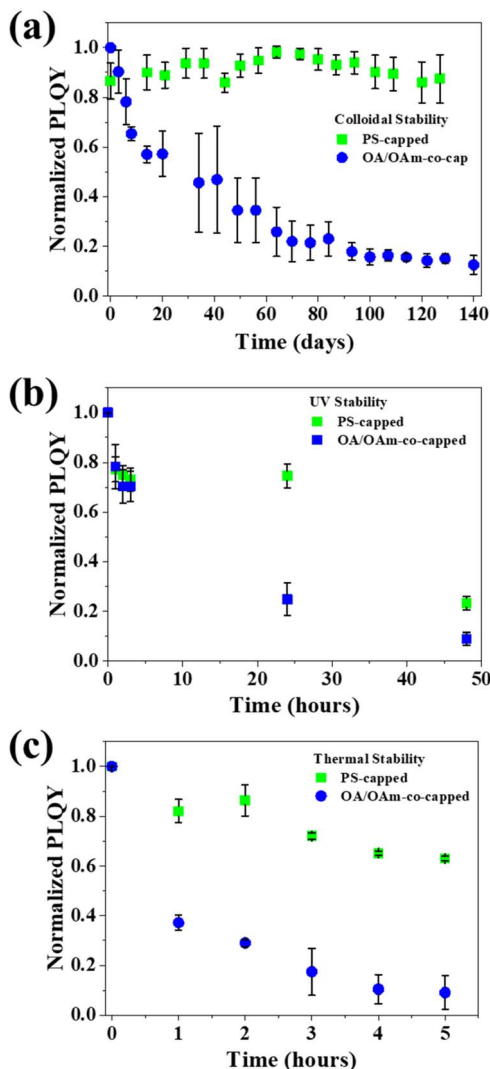


Fig. 5 (a) Colloidal, (b) UV, and (c) thermal (at 80 °C) stabilities of PS-capped and OA/OAm-co-capped  $\text{CsPbBr}_3$  PNCs (control sample) synthesized at optimized conditions ( $Q_{\text{tol}} = 5000 \text{ mL h}^{-1}$  and  $Q_{\text{precursor}} = 60 \text{ mL h}^{-1}$ ).

they can dissociate, leading to PNC agglomeration and quenching of luminescence.<sup>28</sup> This is seen in the sharp decline of PLQY with time. Template-grown PNCs, on the other hand, have PS chains intimately and firmly ligated, ensuring that they maintain their colloidal nature, avoiding agglomeration and preserving their excellent optoelectronic properties. To probe UV stability, both control and templated samples were exposed to 365 nm UV radiation for 48 h. The control OA/OAm-co-capped PNCs experienced a significant PLQY degradation in 24 h, while the templated PNCs retained ~80% of their initial PLQY (Fig. 5b). The decrease in optoelectronic performance can be ascribed to UV-induced photo-oxidation of Pb in PNCs.<sup>63</sup> The superior UV stability of the templated PNCs is likely owing to the outer PS chains on the nanoreactor. The aromatic groups in the chains are known to absorb UV light, which spares the inner perovskite from deleterious effects of UV irradiation.<sup>64</sup> To delve into their thermal stability, the PNCs were exposed to 80 °C for

an extended time. The templated PNCs maintained ~70% of their initial PLQY after 5 h at elevated temperature, while the control decreased to ~40% after 1 h, and then to ~10% after 5 h (Fig. 5c). The considerable increase in PLQY retention can be ascribed to the strongly ligated PS chains on the surface of PNC as discussed above. Unlike the dynamic OA and OAm ligands on the control PNCs, such intimately and vigorously tethered PS chains do not dissociate at elevated temperature, thereby rendering the templated PNCs to maintain their form and ensure high PLQY.<sup>65</sup>

The yield of continuous manufacturing methods is a critical metric that informs the amount of a target material synthesized per time. In our dual-reactor technique (star-like block copolymer nanoreactors inside a flow reactor), the final yield (mass/min) is dependent on the concentration of nanoreactors and perovskite precursors present in the precursor solution. Precursor solutions with higher concentrations of loaded nanoreactors will result in higher yields, whereas lower nanoreactor concentrations will lead to lower yields. In the trials in our study, the concentration of nanoreactors in the precursor solution was kept at a constant 10 mg per 20 mL DMF (perovskite precursors were added in slight excess). At this constant concentration, the calculated yield of  $\text{CsPbBr}_3$  PNCs is  $0.139 \text{ g h}^{-1}$  (eqn S2†). This yield is similar to that previously reported for continuous production of perovskite ( $0.154 \text{ g h}^{-1}$ )<sup>46</sup> and is significantly more than previously reported batch conversion methods ( $0.019 \text{ g h}^{-1}$ ).<sup>46</sup> Notably, the yield of this system scales linearly with the concentration of nanoreactors (eqn S2†). This linear dependence suggests that the yield of the system can be greatly boosted simply by increasing the concentration of loaded nanoreactors. Furthermore, varying the concentration of loaded nanoreactors in the precursor solution will impose insignificant effect on the optical properties of the final PNCs because little change in optical properties was observed as the precursor solution injection rate increased six times (Fig. 3a-c).

## Conclusions

In summary, we have demonstrated the continuous synthesis of highly stable PNCs by incorporating amphiphilic star-like block copolymer nanoreactors into a house-built flow reactor. The antisolvent composition, antisolvent flowrate, and precursor solution flowrate were each systematically optimized to render peak performance of the resultant nanocrystals. Importantly, toluene as an antisolvent, maximized antisolvent flowrate, and  $60 \text{ mL h}^{-1}$  precursor solution flowrate were identified to the ideal parameters. The colloidal, UV, and thermal stabilities of template-grown, PS-capped PNCs produced with these parameters were found to be vastly superior to that of PNCs made with conventional OA and OAm ligands. The strongly and firmly bound PS chains on the surface of PNCs account for enhanced stabilities over those of control samples where OA and OAm ligands are dynamically bonded to the surface. Such a dual-reactor system (nano and flow reactors) enables the markedly improved stabilities of PNCs from the nanoreactor in conjunction with the scaling up rendered by a continuous flow reactor, representing a crucial step towards commercialization of PNCs.



as it overcomes two of the great challenges facing this unique class of material. Future work can be centered on expanding the compositions and emission wavelengths of PNC emitters *via* this dual-reactor system.

## Conflicts of interest

There are no conflicts to declare.

## Acknowledgements

This work is supported by the National Science Foundation (CMMI 1914713).

## Notes and references

- 1 P. Acharyya, K. Maji, K. Kundu and K. Biswas, *ACS Appl. Nano Mater.*, 2020, **3**, 877–886.
- 2 Y. Cao, N. Wang, H. Tian, J. Guo, Y. Wei, H. Chen, Y. Miao, W. Zou, K. Pan, Y. He, H. Cao, Y. Ke, M. Xu, Y. Wang, M. Yang, K. Du, Z. Fu, D. Kong, D. Dai, Y. Jin, G. Li, H. Li, Q. Peng, J. Wang and W. Huang, *Nature*, 2018, **562**, 249–253.
- 3 C. Lan, H. Zou, L. Wang, M. Zhang, S. Pan, Y. Ma, Y. Qiu, Z. L. Wang and Z. Lin, *Adv. Mater.*, 2020, **32**, 2005481.
- 4 C. Chen, L. Gao, W. Gao, C. Ge, X. Du, Z. Li, Y. Yang, G. Niu and J. Tang, *Nat. Comm.*, 2019, **10**, 1–7.
- 5 Q. Chen, J. Wu, X. Ou, B. Huang, J. Almutlaq, A. A. Zhumekenov, X. Guan, S. Han, L. Liang, Z. Yi, J. Li, X. Xie, Y. Wang, Y. Li, D. Fan, D. B. L. Teh, A. H. All, O. F. Mohammed, O. M. Bakr, T. Wu, M. Bettinelli, H. Yang, W. Huang and X. Liu, *Nature*, 2018, **561**, 88–93.
- 6 K. Wang, H. Zhang and Z. J. Gu, *Sci. Bull.*, 2019, **64**, 1205–1206.
- 7 M. Zhang, M. Ye, W. Wang, C. Ma, S. Wang, Q. Liu, T. Lian, J. Huang and Z. Lin, *Adv. Mater.*, 2020, **32**, 2000999.
- 8 B. Wang, M. Zhang, X. Cui, Z. Wang, M. Rager, Y. Yang, Z. Zou, Z. L. Wang and Z. Lin, *Angew. Chem., Int. Ed.*, 2020, **59**, 1611.
- 9 Q. A. Akkerman, M. Gandini, F. Di Stasio, P. Rastogi, F. Palazon, G. Berthoni, J. M. Ball, M. Prato, A. Petrozza and L. Manna, *Nat. Energy*, 2017, **2**, 1–7.
- 10 C.-H. Lu, G. V. Biesold-McGee, Y. Liu, Z. Kang and Z. Lin, *Chem. Soc. Rev.*, 2020, **49**, 4953–5007.
- 11 S. Gonzalez-Carrero, L. Frances-Soriano, M. Gonzalez-Bejar, S. Agouram, R. E. Galian and J. Perez-Prieto, *Small*, 2016, **12**, 5245–5250.
- 12 S. Gonzalez-Carrero, R. E. Galian and J. Perez-Prieto, *J. Mater. Chem. A*, 2015, **3**, 9187–9193.
- 13 F. Liu, Y. Zhang, C. Ding, S. Kobayashi, T. Izuishi, N. Nakazawa, T. Toyoda, T. Ohta, S. Hayase and T. Minemoto, *ACS Nano*, 2017, **11**, 10373–10383.
- 14 S. Bai, Z. Yuan and F. Gao, *J. Mater. Chem. C*, 2016, **4**, 3898–3904.
- 15 M. V. Kovalenko, L. Protesescu and M. I. Bodnarchuk, *Science*, 2017, **358**, 745–750.
- 16 S. Wei, Y. Yang, X. Kang, L. Wang, L. Huang and D. Pan, *Chem. Commun.*, 2016, **52**, 7265–7268.
- 17 H. Huang, M. I. Bodnarchuk, S. V. Kershaw, M. V. Kovalenko and A. L. Rogach, *ACS Energy Lett.*, 2017, **2**, 2071–2083.
- 18 J. Kang and L.-W. Wang, *J. Phys. Chem. Lett.*, 2017, **8**, 489–493.
- 19 S. K. Ha, C. M. Mauck and W. A. Tisdale, *Chem. Mater.*, 2019, **31**, 2486–2496.
- 20 Y. Hassan, O. J. Ashton, J. H. Park, G. R. Li, N. Sakai, B. Wenger, A. A. Haghghirad, N. K. Noel, M. H. Song, B. R. Lee, R. H. Friend and H. J. Snaith, *J. Am. Chem. Soc.*, 2019, **141**, 1269–1279.
- 21 F. Zhang, H. Zhong, C. Chen, X.-g. Wu, X. Hu, H. Huang, J. Han, B. Zou and Y. Dong, *ACS Nano*, 2015, **9**, 4533–4542.
- 22 L. Carbone, C. Nobile, M. De Giorgi, F. Della Sala, G. Morello, P. Pompa, M. Hytch, E. Snoeck, A. Fiore, I. R. Franchini, M. Nadasan, A. F. Silvestre, L. Chiodo, S. Kudera, R. Cingolani, R. Krahne and L. Manna, *Nano Lett.*, 2007, **7**, 2942–2950.
- 23 E. Pedrueza, A. Segura, R. Abargues, J. B. Bailach, J. C. Chervin and J. P. Martínez-Pastor, *Nanotechnology*, 2013, **24**, 205701.
- 24 Z. Kang, A. A. Banishev, G. Lee, D. A. Scripka, J. Breidenich, P. Xiao, J. Christensen, M. Zhou, C. J. Summers, D. D. Dlott and N. N. Thadhani, *J. Appl. Phys.*, 2016, **120**, 043107.
- 25 I. C. Smith, E. T. Hoke, D. Solis-Ibarra, M. D. McGehee and H. I. Karunadasa, *Angew. Chem., Int. Ed.*, 2014, **126**, 11414–11417.
- 26 Y. Lin, Y. Bai, Y. Fang, Z. Chen, S. Yang, X. Zheng, S. Tang, Y. Liu, J. Zhao and J. Huang, *J. Phys. Chem. Lett.*, 2018, **9**, 654–658.
- 27 F. Bella, G. Griffini, J.-P. Correa-Baena, G. Saracco, M. Grätzel, A. Hagfeldt, S. Turri and C. Gerbaldi, *Science*, 2016, **354**, 203–206.
- 28 J. De Roo, M. Ibáñez, P. Geiregat, G. Nedelcu, W. Walravens, J. Maes, J. C. Martins, I. Van Driessche, M. V. Kovalenko and Z. Hens, *ACS Nano*, 2016, **10**, 2071–2081.
- 29 J. Song, J. Li, X. Li, L. Xu, Y. Dong and H. Zeng, *Adv. Mater.*, 2015, **27**, 7162–7167.
- 30 I. Levchuk, A. Osvet, X. Tang, M. Brandl, J. D. Perea, F. Hoegl, G. J. Matt, R. Hock, M. Batentschuk and C. J. Brabec, *Nano Lett.*, 2017, **17**, 2765–2770.
- 31 D. N. Dirin, L. Protesescu, D. Trummer, I. V. Kochetygov, S. Yakunin, F. Krumeich, N. P. Stadie and M. V. Kovalenko, *Nano Lett.*, 2016, **16**, 5866–5874.
- 32 A. Loiudice, S. Saris, E. Oveisi, D. T. Alexander and R. Buonsanti, *Angew. Chem., Int. Ed.*, 2017, **56**, 10696–10701.
- 33 Y. Chang, Y. J. Yoon, G. Li, E. Xu, S. Yu, C.-H. Lu, Z. Wang, Y. He, C. H. Lin, B. K. Wagner, V. V. Tsukruk, Z. Kang, N. Thadhani, Y. Jiang and Z. Lin, *ACS Appl. Mater. Interfaces*, 2018, **10**, 37267–37276.
- 34 S. Liang, M. Zhang, G. M. Biesold, W. Choi, Y. He, Z. Li, D. Shen and Z. Lin, *Adv. Mater.*, 2021, **33**, 2005888.
- 35 Y. He, Y. J. Yoon, Y. W. Harn, G. V. Biesold-McGee, S. Liang, C. H. Lin, V. V. Tsukruk, N. Thadhani, Z. Kang and Z. Lin, *Sci. Adv.*, 2019, **5**, eaax4424.
- 36 Y. J. Yoon, Y. Chang, S. Zhang, M. Zhang, S. Pan, Y. He, C. H. Lin, S. Yu, Y. Chen, Z. Wang, Y. Ding, J. Jung,



N. Thadhani, V. V. Tsukruk, Z. Kang and Z. Lin, *Adv. Mater.*, 2019, 1901602, DOI: [10.1002/adma.201901602](https://doi.org/10.1002/adma.201901602).

37 S. Pan, Y. Chen, Z. Wang, Y.-W. Harn, J. Yu, A. Wang, M. J. Smith, Z. Li, V. V. Tsukruk and J. Peng, *Nano Energy*, 2020, **77**, 105043.

38 Y. Liu, J. Wang, M. Zhang, H. Li and Z. Lin, *ACS Nano*, 2020, **14**, 12491–12521.

39 X. Pang, L. Zhao, W. Han, X. Xin and Z. Lin, *Nat. Nanotechnol.*, 2013, **8**, 426–431.

40 R. W. Epps, K. C. Felton, C. W. Coley and M. Abolhasani, *Lab Chip*, 2017, **17**, 4040–4047.

41 I. Lignos, S. Stavrakis, G. Nedelcu, L. Protesescu, A. J. Demello and M. V. Kovalenko, *Nano Lett.*, 2016, **16**, 1869–1877.

42 R. M. Maceiczyk, K. Dümbgen, I. Lignos, L. Protesescu, M. V. Kovalenko and A. J. deMello, *Chem. Mater.*, 2017, **29**, 8433–8439.

43 Y. H. Song, S. H. Choi, W. K. Park, J. S. Yoo, S. B. Kwon, B. K. Kang, S. R. Park, Y. S. Seo, W. S. Yang and D. H. Yoon, *Sci. Rep.*, 2018, **8**, 1–6.

44 X. Liang, R. W. Baker, K. Wu, W. Deng, D. Ferdani, P. S. Kubiak, F. Marken, L. Torrente-Murciano and P. J. Cameron, *React. Chem. Eng.*, 2018, **3**, 640–644.

45 C. Li, B. Ding, L. Zhang, K. Song and S. Tao, *J. Mater. Chem. C*, 2019, **7**, 9167–9174.

46 G. M. Biesold, S. Liang, B. K. Wagner, Z. Kang and Z. Lin, *Nanoscale*, 2021, **13**, 13108–13115.

47 S. Liang, M. Zhang, Y. He, Z. Kang, M. Tian, M. Zhang, H. Miao and Z. Lin, *Chem. Mater.*, 2021, **33**, 6701–6712.

48 H. Hu, J. Saniger, J. Garcia-Alejandre and V. Castaño, *Mater. Lett.*, 1991, **12**, 281–285.

49 X. Pang, Y. He, J. Jung and Z. Lin, *Science*, 2016, **353**, 1268–1272.

50 Y. Wang, J. He, H. Chen, J. Chen, R. Zhu, P. Ma, A. Towers, Y. Lin, A. J. Gesquiere and S. T. Wu, *Adv. Mater.*, 2016, **28**, 10710–10717.

51 I. M. Smallwood, *Handbook of Organic Solvent Properties*, 1st edn, 1996.

52 H. Huo, K. Li, Q. Wang and C. Wu, *Macromolecules*, 2007, **40**, 6692–6698.

53 A. Darbyshire and T. Mullin, *J. Fluid Mech.*, 1995, **289**, 83–114.

54 K. V. Sharp and R. J. Adrian, *Exp. Fluids*, 2004, **36**, 741–747.

55 K. D. Nagy, B. Shen, T. F. Jamison and K. F. Jensen, *Org. Process Res. Dev.*, 2012, **16**, 976–981.

56 D. Esparza, S. Sidhik, T. López-Luke, J. M. Rivas and E. De la Rosa, *Mater. Res. Express*, 2019, **6**, 045041.

57 Q. Han, W. Wu, W. Liu and Y. Yang, *RSC Adv.*, 2017, **7**, 35757–35764.

58 J. H. Heo, J. K. Park and S. H. Im, *Cell Rep. Phys. Sci.*, 2020, **1**, 100177.

59 Y.-H. Kim, H. Cho and T.-W. Lee, *Proc. Natl. Acad. Sci. U. S. A.*, 2016, **113**, 11694–11702.

60 A. L. Rogach, *Sci. Bull.*, 2017, **62**, 314–315.

61 J. Woo Choi, H. C. Woo, X. Huang, W.-G. Jung, B.-J. Kim, S.-W. Jeon, S.-Y. Yim, J.-S. Lee and C.-L. Lee, *Nanoscale*, 2018, **10**, 13356–13367.

62 Y. Xu, W. Li, F. Qiu and Z. Lin, *Nanoscale*, 2014, **6**, 6844–6852.

63 J. Li, L. Wang, X. Yuan, B. Bo, H. Li, J. Zhao and X. Gao, *Mater. Res. Bull.*, 2018, **102**, 86–91.

64 T. Li, C. Zhou and M. Jiang, *Polym. Bull.*, 1991, **25**, 211–216.

65 X. Yuan, X. Hou, J. Li, C. Qu, W. Zhang, J. Zhao and H. Li, *Phys. Chem. Chem. Phys.*, 2017, **19**, 8934–8940.

